Ultrasound-Modulated Two-Fluid Atomization of a Water Jet

Shirley C. Tsai, Paul Childs, and Patrick Luu
Dept. of Chemical Engineering, California State University, Long Beach, CA 90840

A new spray technique, called ultrasound-modulated two-fluid (UMTF) atomization, is based on resonance between the liquid capillary waves generated by ultrasound and those generated by high-velocity air. The capillary waves generated by ultrasound on the cone of liquid film issuing from a coaxial two-fluid atomizer are magnified in amplitude by air blowing around them. Atomization occurs when the amplitude of the capillary waves is too great to maintain wave stability, and the resulting drop sizes are determined by the frequency of the ultrasound. Calculations of the relative amplitude growth for the capillary waves of various wavelengths yield predictions that agree remarkably well with experimental results of drop size and size distribution. Specifically, uniform drops with diameter determined by the third harmonic frequency of the ultrasound are obtained in UMTF atomization at high air velocity and large air-to-water mass ratio. In contrast, drop-size distributions with multiple peaks are obtained in UMTF atomization at low air velocity and small air-to-water mass ratio. The use of air also allows the liquid jet to atomize at ultrasonic power levels below and liquid flow rates above the threshold values for ultrasonic atomization without air. These new findings provide not only direct evidence of the capillary wave mechanism but also a means of controlling drop size and size distribution in two-fluid atomization.

Introduction

Airblast or two-fluid atomization has been widely used in slurry combustion and spray drying (Marshall, 1954; Dombrowski and Johns, 1963; Laskowski and Ranz, 1970). Two-fluid atomizers have a number of advantages over pressure atomizers, including lower slurry pressure and finer spray. The wave nature of two-fluid atomization was verified by direct wavelength and frequency measurements of a liquid jet issuing from a coaxial research atomizer (Eroglu and Chigier, 1991). Nevertheless, the physical mechanisms of this complex process are not yet fully understood. Drop sizes are related to atomizer designs and atomization conditions through empirical correlations (Lefebvre, 1989). In contrast, the capillary wave mechanism of ultrasonic atomization (atomization of liquid using ultrasound alone) of a liquid jet has been well accepted since its first demonstration in 1962 (Lang, 1962; Berger, 1985; Elrod et al., 1989; Lin and Woods, 1991). Specifically, capillary waves are formed in liquid film introduced onto a solid surface that is vibrating at frequencies in excess of 10 kHz; an increase in the vibrational amplitude results in a corresponding increase in the amplitude of the liquid capillary waves (Berger, 1985). Atomization occurs when the vibration amplitude increases to the point where the amplitude of the capillary waves is too great to maintain wave stability. The resulting drop size is proportional to the wavelength of the capillary waves which is, in turn, determined by the ultrasonic frequency in accordance with the Kelvin equation (Lang, 1962).

Capillary waves are also produced on the surface of a liquid jet by blowing air around it as in two-fluid atomization (Jeffreys, 1925; Adelberg, 1967 and 1968; Tsai and Viers, 1992). We believe that when the liquid capillary waves generated by air are in resonance with those generated by a vibrating nozzle, energy is transferred from the air to the liquid jet, resulting in jet atomization. In other words, the capillary waves created on the surface of the liquid jet by a vibrating nozzle are magnified in amplitude by the air blowing around them and eventually collapse into drops. We call this new spray technique "ultrasound-modulated two-fluid (UMTF) atomization" (Tsai, 1995). The theoretical basis and experimental verification of drop size and size distribution resulting

from break up of such resonant liquid capillary waves are given in this article. Remarkable agreement between the theoretical predictions and the experimental results led us to conclude that two-fluid atomization of a liquid jet, at least in part, occurs via the same capillary wave mechanism as the ultrasonic atomization.

Also presented in this article is a brief discussion of the well-studied dispersion relations based on the linearized Navier–Stokes equations for spatial instability (Leib and Goldstein, 1986; Lin and Lian, 1993) and temporal instability of a liquid jet (Reitz and Bracco, 1982; Lin and Ibrahim, 1990), as well as the unified theory on break up of a liquid jet issuing from a nozzle into the atmosphere (Lin and Lian, 1990). Comparison of these dispersion relations to our experimental results is limited because of the differences in atomization conditions.

Experimental Setup

A diagram of the bench-scale atomization unit is shown in Figure 1. Major components of the unit include an atomization chamber, a coaxial two-fluid atomizer, Brooks precision rotameters for accurate flow-rate measurement, and a Malvern Particle Sizer 2600c for spray-size analysis. The atomization chamber (Tsai and Viers, 1992) measures 35.5 cm $\times$35.5 cm$\times$64 cm. The coaxial two-fluid atomizer is located at the center of the atomization chamber, as shown in Figure 1. It consists of a Sono-Tek ultrasonic atomizing nozzle system Model 8700 (Berger, 1991) for liquid flow and an annulus that allows air blowing around the liquid jet as it exits the nozzle tip in a manner similar to an externally mixed two-fluid atomizer (Tsai and Viers, 1992). The distance between the nozzle tip and the optical path (abbreviated as distance or noz-beam in the figures) was varied from 2.3 cm to 16.5 cm.

The Sono-Tek ultrasonic nozzle (Berger, 1985) as shown in Figure 2 consists of a pair of washer-shaped ceramic piezoelectric transducers sandwiched between two titanium cylinders located in the large diameter (about 3.6 cm) of the nozzle body. Two O-rings serve to isolate the nozzle from the external housing. The piezoelectric transducers receive electrical input in the form of a high-frequency signal from a power generator Model PS-88 and convert the input electrical energy into mechanical energy of vibration. The nozzle is geometrically configured such that excitation of the piezoelectric transducers create a standing wave through the nozzle with maximum vibration amplitude occurring at the nozzle tip (orifice diameter of 0.93 ± 0.02 mm) and a node at the fixed joint of the piezoelectric transducers, as shown in Figure 2. The input electric power to the piezoelectric transducers can be varied from zero to 10 W as measured by a power meter, and the corresponding signal as measured by a Tektronix digitized oscilloscope Model TDS-460 is shown in Figure 3. The frequency spectrum of the Sono-Tek ultrasonic nozzle #1 (Erickson, 1987) as measured by a Hewlett-Packard Spectrum Analyzer Model 8562A shows fundamental (first harmonic) resonant frequency of the piezoelectric transducers at 54 kHz and the third harmonic frequency of 174 kHz, as shown in Figure 4; the relative spectral power (square of voltage) of the third harmonic with respect to the fundamental varies from 0.78 (-1.1 dB$_m$) to 0.29 (-5.3 dB$_m$). The fifth (290 kHz) and the seventh harmonics also exist, but to a

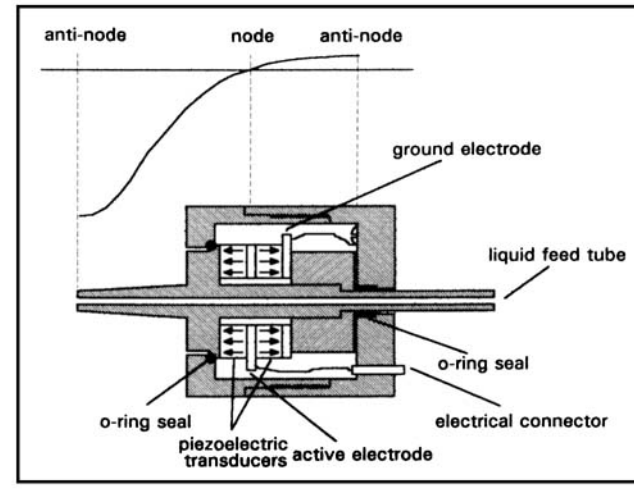

Figure 2. Sono-Tek ultrasonic atomizing nozzle.

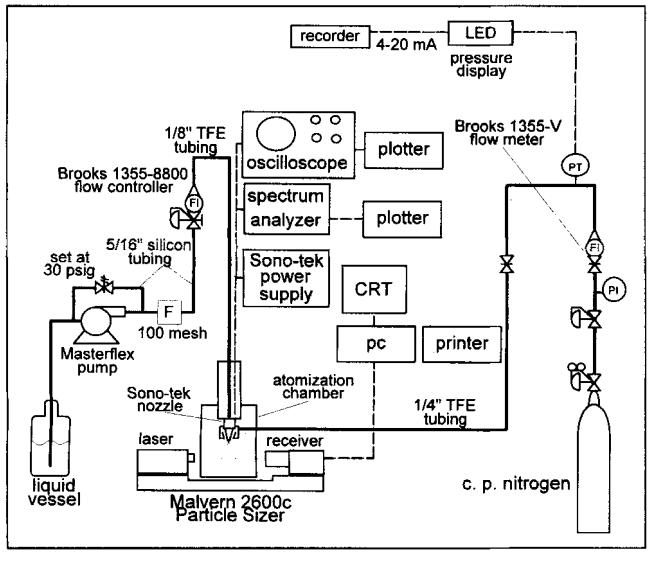

Figure 1. Bench-scale atomization setup.

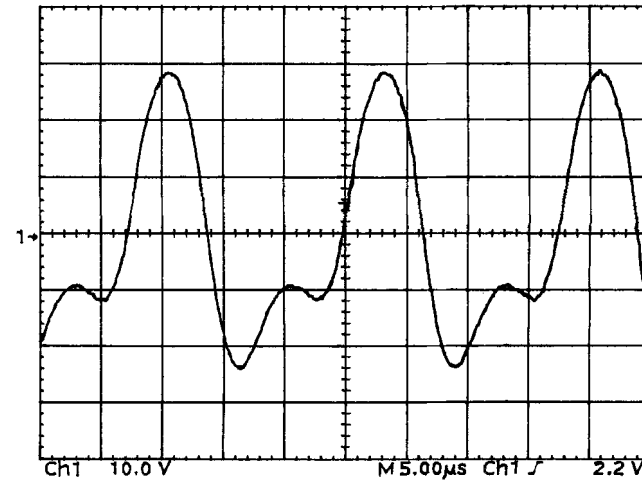

Figure 3. Electrical signal at the input to the Sono-Tek ultrasonic atomizing nozzle #1.

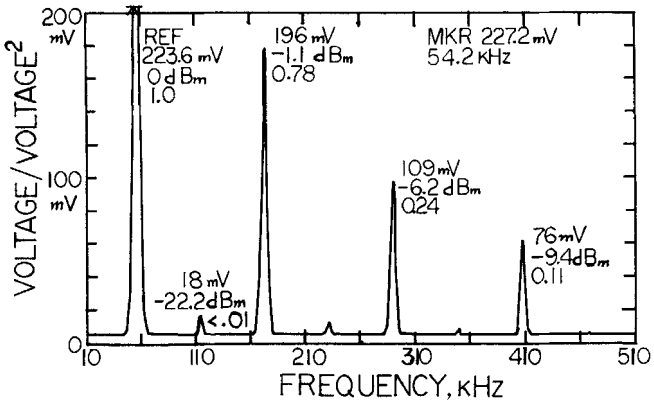

Figure 4. Frequency response of the Sono-Tek ultrasonic nozzle (#1) system Model 8700 with input signal at 54 kHz (fundamental resonance frequency of the transducer).

much lesser degree. Note that the vertical scale in Figure 4 is linear in mV only. Likewise, the frequency spectrum of the Sono-Tek ultrasonic nozzle #2 shows the first three harmonics at frequencies of 108 kHz, 336 kHz, and 560 kHz. Even harmonics are negligible in both nozzles. The relative spectral power levels of the higher harmonics with respect to that of the fundamental depend on the driving electrical circuit of the nozzle system.

A steady liquid flow rate is maintained by a diaphragm-type Brooks Flow Controller Model 8800 that is an integral part of the precision rotameter for liquid-flow-rate measurement. Most experiments were carried out at constant water flow rates of 17.3 and 5.1 cm^3/min, equivalent to liquid velocities of 42 ± 2 and 12 ± 2 cm/s. A water flow rate as low as 1.3 cm^3/min was also used in an attempt to achieve the mean drop diameter reported in the literature (Berger, 1985). Constant air flow rates ranging from 28.6 to 7.2 Standard L/min provide air velocities ranging from 220 ± 30 to 80 ± 5 m/s. The large uncertainty in air velocity is caused by errors in measurement of the annular cross-sectional area for air flow.

The atomized drop size and size distribution is measured using a Malvern Particle Sizer Model 2600c and presented in frequency (i.e., volume percent) plots of drop diameters (Model Independent). The Malvern Particle Sizer measures the drop size and size distribution of the spray through diffractive scattering (Fraunhofer diffraction) of laser light (Swithenbank et al., 1976). This line-of-sight measurement takes a 13-s time average of a steady-state spray, and covers the larger drops at the rim and the smaller drops in the core of the spray as observed by the point measurement of Phase Doppler Interferometry (McDonell and Samuelsen, 1993). The frequency plot is volume based, but the number-based mean diameter (NMD) is also available in the Malvern software. Based on our results of unimodal (single-peak) drop-size distributions, the NMD is significantly smaller than the peak diameter of the volume-based frequency plot because larger drops carry more weight than smaller drops in the latter, while the reverse is true in the former. The Particle Sizer is calibrated using known particle-size and size-distribution standards provided by Advanced Particle Measurement, California. The uncertainty in drop-size measurement is $\pm5\%$. For example, the standard deviation of the volume-mean diameters of the drop-size distributions in ultrasound-modulated two-fluid atomization is ±2 μm. Excellent reproducibility has been obtained, as shown by the open and solid data points of duplicate experiments in the volume-percent plots in the Results and Discussion Section.

Resonant Liquid Capillary Waves Mechanism

When air blows along a liquid jet, waves form on the jet surface. The amplitude (A) of these surface waves is described by the following differential equation (Jeffreys, 1925; Adelberg, 1967, 1968; Tsai and Viers, 1992):

$$\frac{\partial A}{\partial t} = A\left[\frac{\pi\beta\rho_A(V_A-u)^2}{\lambda\rho u} - \frac{8\pi^2\mu}{\rho\lambda^2}\right] = A\zeta, \qquad (1)$$

where λ, u, ρ, ρ_A, μ, and β are wavelength, wave velocity, liquid density, air density, liquid viscosity, and Jeffreys sheltering parameter, respectively. Note that β is a numerical value ranging from 0 to 1 that represents the fraction of waves exposed to wind (Jeffreys, 1925). Equation 1 was first derived (Jeffreys, 1925) for wind blow over water surface from the equations of continuity and motion with two assumptions: (1) the tangential stress is zero at the air–water interface, and (2) the pressure of the wind with a relative velocity V_A-u on the advancing wave profile roughly equals $\beta\rho_A(V_A-u)^2\partial A/\partial z$, where the z-axis is the direction of wind blow. It was later (Adelberg, 1967) applied to break up of a liquid jet in a gas stream flowing parallel to the jet axis (z-axis). These surface waves are standing waves with the amplitude proportional to $e^{\zeta t}\cos(2\pi z/\lambda)$. The amplitude at a fixed z grows exponentially with time when V_A exceeds the minimum values determined by setting $\partial A/\partial t = 0$, that is, $\zeta = 0$.

From Eq. 1, we see that the amplitude that is damped by the liquid viscous force increases as the relative air velocity (V_A-u) increases. When both the aerodynamic pressure and the surface tension (σ) are significant, the wave velocity u is given (Jeffreys, 1925) by

$$u = \left[\frac{\lambda\Lambda}{2\pi} + \frac{2\pi\sigma}{\lambda\rho}\right]^{1/2}, \qquad (2)$$

where the acceleration (Λ) is caused by the aerodynamic drag on the liquid jet. The first term, due to acceleration waves, is neglected in comparison with the second term, due to capillary waves, for pertinent λ's under investigation. Our order-of-magnitude calculations (Tsai and Viers, 1992) show that at an air velocity of 250 m/s, the first term is less than one-fifth of the second term for water waves with λ's smaller than 100 μm. This is also true for water waves with λ's smaller than 250 μm at an air velocity of 100 m/s.

When in resonance, λ of the air-generated waves equals the wavelength λ_C of the capillary waves generated on a liquid jet vibrating at an ultrasonic frequency (f in cps or Hz) in accordance with the Kelvin equation (Lang, 1962):

$$\lambda_c = \left[\frac{8\pi\sigma}{\rho f^2}\right]^{1/3}. \qquad (3)$$

Table 1. Minimum Air Velocity for Temporal Amplitude Growth of the Capillary Waves

λ_C, μ	18	25	28	39	54	85	150	300
f, kHz	560	336	290	174	108	54	23	8
V_A^{min}, m/s	142	110	102	80	63	45	30	18

The wave velocity u equals $(2\pi\sigma/\lambda_C \rho)^{1/2}$. Note that a liquid jet issuing from an ultrasonic nozzle is forced to vibrate at the same frequency as the ultrasound, but the frequency of the capillary waves generated is only half of the ultrasonic frequency (Lang, 1962). When the capillary waves generated on the vibrating liquid jet are in resonance with the capillary waves generated by the blowing air, energy is transferred from the air to the liquid jet. As a result, the amplitude of the liquid capillary waves grows exponentially with time, that is, $A = A_o e^{\zeta t}$ as obtained by integration of Eq. 1, when V_A exceeds the minimum values. These minimum air velocities for capillary waves with wavelengths longer than 40 μm are equal to or less than 80 m/s, as shown in Table 1. Atomization occurs when the wave amplitude is too great to maintain wave stability.

Results and Discussion

Based on the aforementioned resonance theory, ultrasound can be used upstream (before the liquid jet is impinged upon by air) to generate liquid capillary waves with wavelengths determined by its frequencies, and thus control the drop size and size distribution in two-fluid atomization. We call this novel spray technique "ultrasound-modulated two-fluid (UMTF) atomization" (Tsai, 1995).

Ultrasonic atomization (no air)

Atomization of a water jet was first carried out at water flow rates of 1.3, 5.1, and 17.3 cm^3/min using ultrasound alone to ensure that the Sono-Tek ultrasonic nozzle system was indeed functional. At input power levels above minimum values, soft sprays with a round top were seen to start immediately at the nozzle tip. We found that the minimum power levels required to sustain stable ultrasonic atomization varied with water flow rates. The minimum power requirements of nozzle #1 (54 kHz fundamental frequency) are 1.0, 1.8, and 1.9 W at water flow rates of 1.3, 5.1, and 17.3 cm^3/min, respectively. Power levels up to 3.5 W have no significant effect on the drop-size distribution in ultrasonic atomization.

The drop-size distribution obtained at a water flow rate of 1.3 cm^3/min and a nozzle tip-to-laser beam distance of 2.5 cm has a peak volume percent at a drop diameter of 50 μm (Figure 5). The corresponding volume mean diameter (VMD) is 50 ± 2 μm and the NMD is 36 ± 2 μm, which is somewhat larger than the reported number median diameter of 29 μm obtained at 12 cm^3/min water rate (Berger, 1985). This discrepancy may be attributable in part to the difference between the number mean diameter and the number median diameter. The drop-size distribution degenerates into two peaks: a primary peak at 40-μm drop diameter and a shoulder at 85 μm as the nozzle-to-beam distance increases to 13.5 cm.

Figure 6 shows that as the water flow rate increases to 5.1 cm^3/min, the drop-size distribution measured at a nozzle-to-beam distance of 2.5 cm shows a dominant peak at 70 μm drop diameter (VMD of 61 ± 2 μm and NMD of 41 ± 2 μm). It degenerates into a primary peak at 80 μm and a shoulder at 40 μm as the nozzle-to-beam distance increases to 13.5 cm; further increase in the nozzle-to-beam distance from 13.5

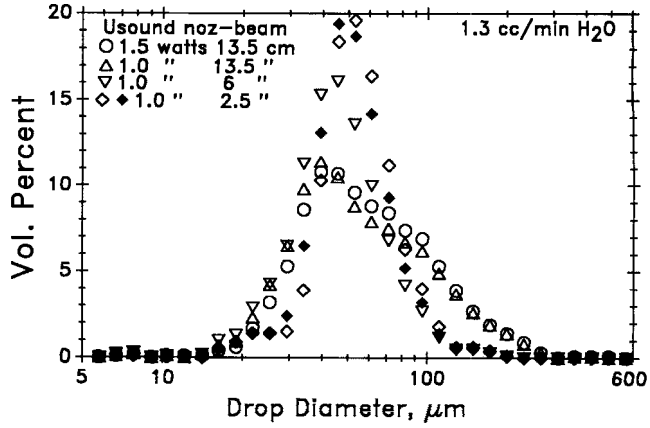

Figure 5. Atomization of water jet at velocity of 3 ± 0.5 cm/s (1.3 cm^3/min) by ultrasound alone.

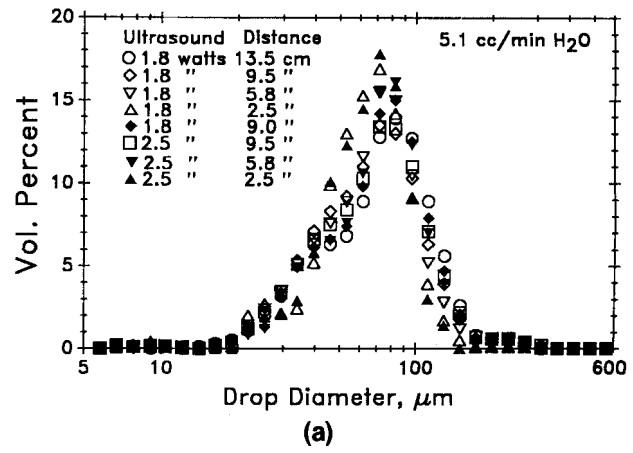

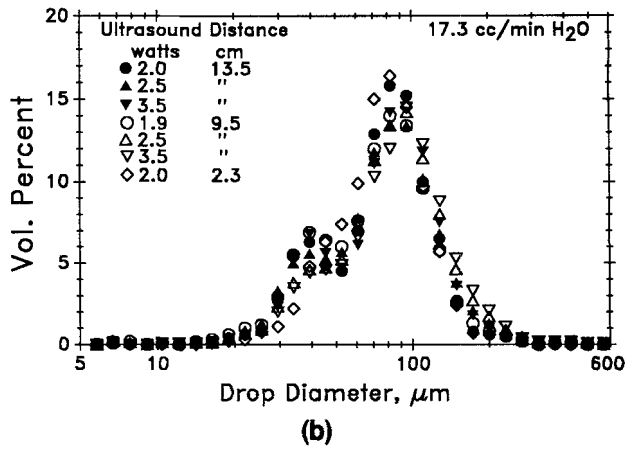

Figure 6. Atomization of water jet at velocity of: (a) 12 ± 2 cm/s (5.1 cm^3/min water flow rate) by ultrasound alone; (b) 42 ± 2 cm/s (17.3 cm^3/min water flow rate) by ultrasound alone.

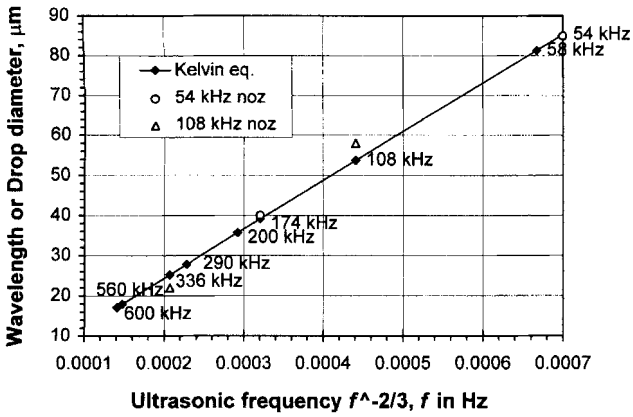

Figure 7. Drop diameters vs. capillary wavelengths calculated in accordance with Kelvin equation.

to 16.5 cm has no significant effect on the drop-size distribution. Also shown in Figure 6 is that the shoulder at 40 μm becomes more distinct, and the primary peaks shifts from 80 μm to 85 μm as the water flow rate increases to 17.3 cm^3/min; varying the nozzle-to-beam distance from 2.3 to 13.5 cm has little effect on the drop-size distribution.

The two peaks at 40 μm and 80–85 μm diameters of the aforementioned drop-size distributions can be attributed to break up of the capillary waves generated by the first harmonic (54 kHz) and the third harmonic (174 kHz) of the ultrasound from nozzle #1. It should be noted that the frequency ratio of the capillary waves with wavelengths of 85 μm and 40 μm based on the Kelvin formula, Eq. 3, equals $(85/40)^{3/2} = 3$. No third peak is seen in the drop-size distributions despite the presence of the fifth and seventh harmonics in the frequency-response curve of the ultrasonic nozzle (see Figure 4). This is not surprising in light of the much lower power levels of these higher harmonics and the considerably more surface energy required to produce drops 28 μm in diameter and smaller. Likewise, two-peak drop-size distributions were also obtained in ultrasonic atomization at a water flow rate of 12 cm^3/min using nozzle #2 (fundamental frequency of 108 kHz). As expected, the primary peak shifts from 80–85 μm to 58 ± 2 μm, and the secondary peak from 40 μm to 22 μm because nozzle #2 has higher harmonic frequencies than nozzle #1. In fact, as shown in Figure 7, these peak drop diameters coincide with the wavelengths of the capillary waves calculated by the Kelvin formula, Eq. 3. It should be noted that the volume-based peak diameter is in general larger than the NMD. For example, the volume-based drop-size distribution with 40 μm peak shown in Figure 8(b) has an NMD of 20 μm, which is half of the wavelength of the capillary waves generated by the third harmonic of ultrasound from nozzle #1.

Effects of ultrasound on two-fluid atomization

In UMTF atomization, a water jet issues from a coaxial two-fluid atomizer whose nozzle tip vibrates at an ultrasonic frequency; it is then impinged upon by air blowing around it. Nozzle #1 with first- (fundamental) and third-harmonic frequencies of 54 kHz and 174 kHz was used in this study. The resulting cone-shape sprays are similar to those in two-fluid

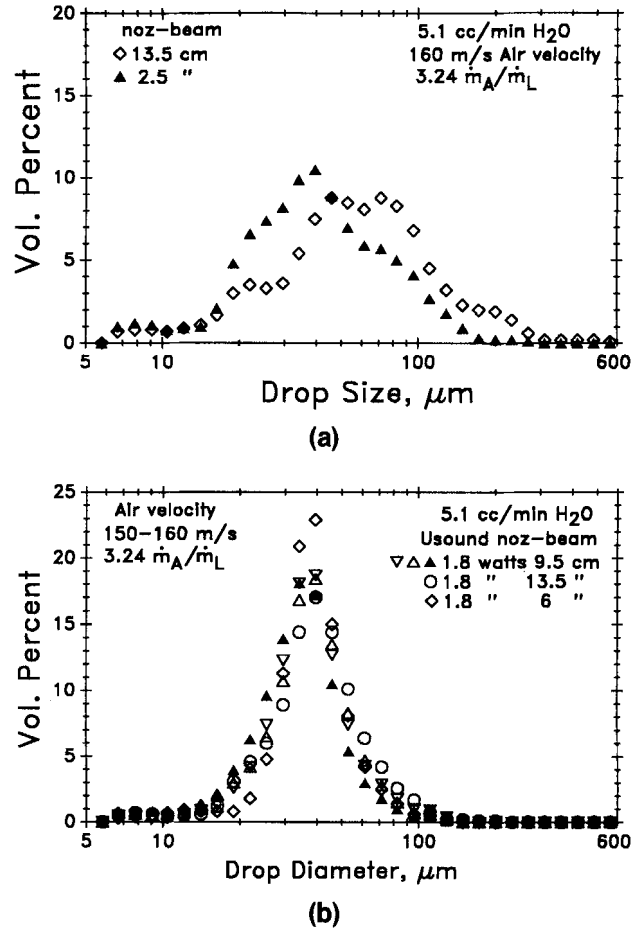

Figure 8. (a) Two-fluid atomization of water jet at velocity of 12 ± 2 cm/s (5.1 cm^3/min water flow rate) and 160 m/s air velocity (air-to-water mass ratio of 3.24); (b) UMTF atomization of water jet at velocity of 12 ± 2 cm/s (5.1 cm^3/min water flow rate), 150–160 m/s air velocity (air-to-water mass ratio of 3.24), and 1.8 W ultrasound power input.

atomization (Lefebvre, 1989; Tsai and Viers, 1992). However, the drop-size distribution is considerably narrowed and shifted to smaller drop diameters compared to that of two-fluid atomization (see Figures 8 to 10). Comparisons of Figure 8b and Figure 9a to Figure 6a reveal that the peak volume percent occurs at the drop diameter (40 μm) generated by the third-harmonic frequency with wavelength of 39 μm. In other words, unimodal drop-size distributions (half-widths of 15 to 20 μm) with peak volume percent at 40 μm drop diameter (VMD of 35 ± 2 μm and NMD of 20 ± 2 μm) and excellent reproducibility are seen in Figure 8b and Figure 9a for UMTF atomization of 5.1 cm^3/min water using ultrasound at input power ranging from 1.5 to 2.5 W, and air at a velocity of 150–160 m/s and air-to-water mass ratio of 3.24. Figure 9a also shows that the ultrasound input power can be as low as 1.0 W when air velocity is increased to 200 m/s and air-to-water mass ratio to 4.73. Furthermore, we found that the nozzle-to-beam distance varying from 2.3 to 13.5 cm had no effect on the drop-size distribution because of a single

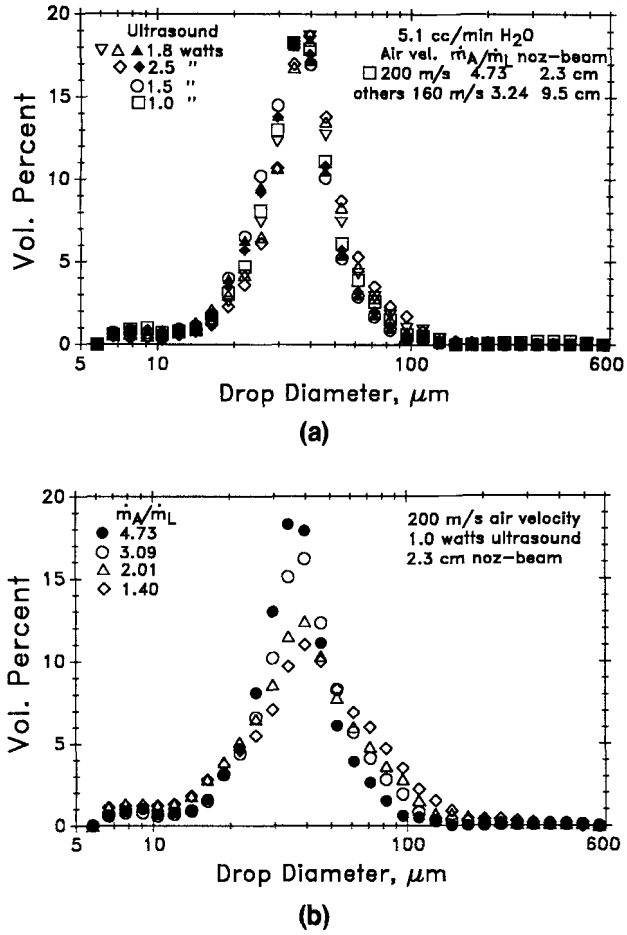

Figure 9. (a) Effects of ultrasound input power on the drop-size distribution of UMTF atomization of water jet at velocity of 12±2 cm/s (5.1 cm³/min water flow rate) and 150–160 m/s air velocity (air-to-water mass ratio of 3.24); (b) effects of air-to-water mass ratio on the drop size and size distribution in UMTF atomization at 200 m/s air velocity and 1.0 W ultrasound power.

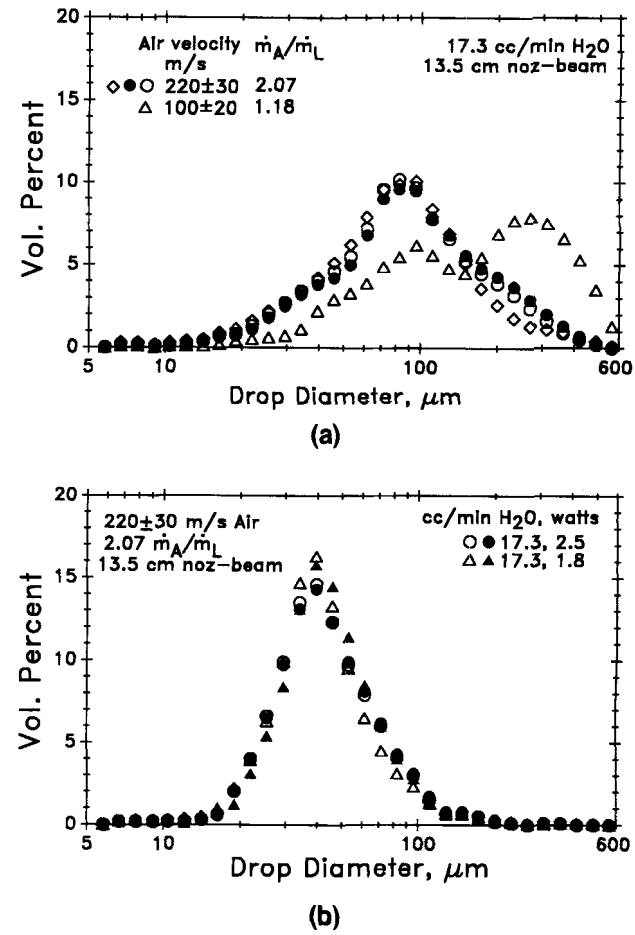

Figure 10. (a) Two-fluid atomization of water jet at velocity of 42±2 cm/s (water flow rate of 17.3 cm³/min) and air velocities of 100±20 and 220±30 m/s; (b) UMTF atomization of water jet at velocity 42±2 cm/s (water flow rate of 17.3 cm³/min), air velocity of 220±30 m/s (air-to-water mass ratio of 2.07), and ultrasound input power levels of 1.8 and 2.5 W.

predominating wavelength. Increase in air-to-water mass ratio from 3.24 to 7.02 had no effect on the drop-size distribution either. It should be noted that in the presence of high-velocity air, water at a flow rate of 5.1 cm³/min was atomized even at 1.0 W, resulting in drop-size distributions similar to those obtained at 1.8 and 2.5 W (see Figure 9a); no atomization was observed at this water flow rate when ultrasound at 1.5 W was used alone. In other words, the capillary waves generated by 1.0 W ultrasonic energy were stable with no air flow, but were unstable and broke up into sprays with air flow at a high velocity.

Similar results were obtained in UMTF atomization of water at 17.3 cm³/min flow rate and ultrasound input power of 2.5 or 1.8 W. Specifically, drop-size distributions with one slightly broader peak at 40 μm diameter (VMD of 44±2 μm, NMD of 28±2 μm, and half-width of 30 μm) and excellent reproducibility are seen in Figure 10b for UMTF atomization at 220±30 m/s air velocity and air-to-water mass ratio of 2.07. However, as the air velocity is reduced from 220±30 m/s to 100±20 m/s and the air-to-water mass ratio from 2.07 to 1.18, drop-size distributions with three distinct peaks at about 40 μm, 90 μm, and 300 μm are seen in Figure 11a despite fine-tuning of the nozzle position with respect to the position of air impingement. Comparisons of Figure 11a to Figure 10a and Figure 6b clearly show that the drop-size distributions in Figure 11a are composed of those of ultrasonic atomization and two-fluid atomization. In fact, the drop-size distribution obtained at these conditions (low air velocity and low air-to-water mass ratio) varies with the ultrasonic power. As shown in Figure 11b, the larger drops generated by air gain importance as the ultrasonic input power decreases.

We believe that the predominating 40 μm peak of the drop-size distribution for UMTF atomization at high air velocities and large air-to-water mass ratios is attributable to two effects: (1) resonance between the liquid capillary waves generated by the ultrasound and those generated by the

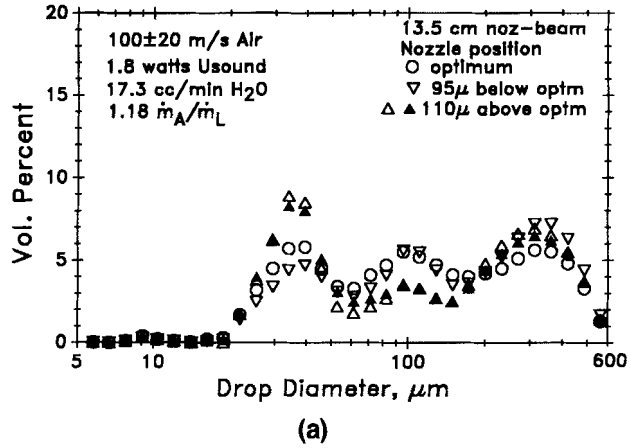

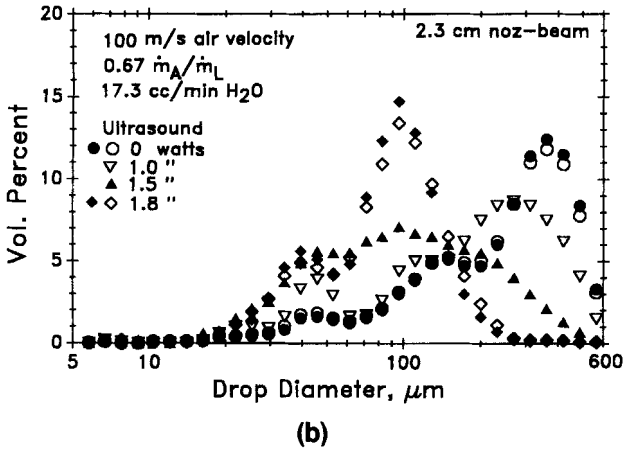

Figure 11. UMTF atomization of water jet at water velocity of 42±2 cm/s (17.3 cm³/min water flow rate): (a) air velocity of 100±20 m/s (air-to-water mass ratio of 1.18), and ultrasound input power levels of 1.8 W; (b) air velocity of 100 m/s (air-to-water mass ratio of 0.67), but various ultrasound input power levels.

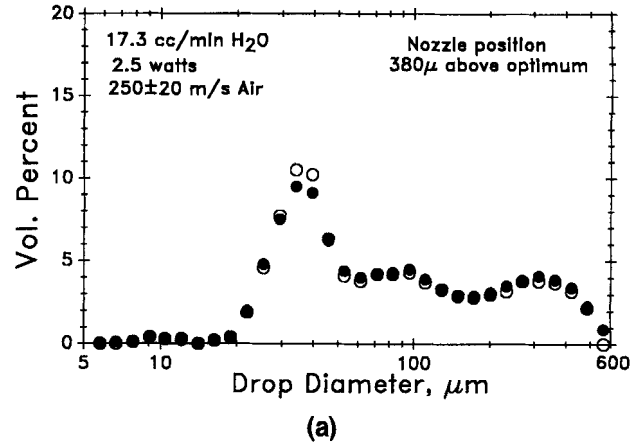

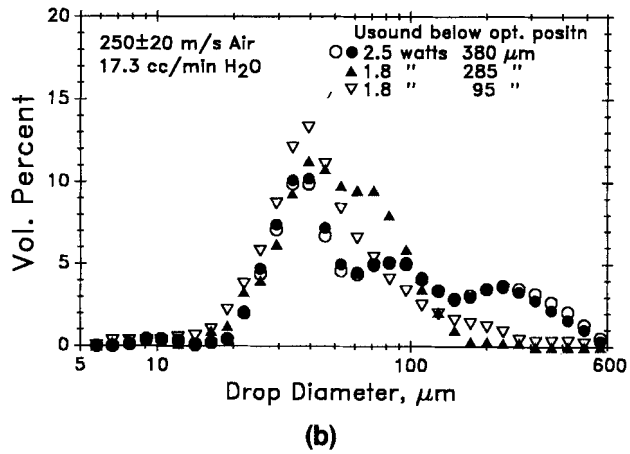

Figure 12. UMTF atomization of water jet at water velocity of 42±2 cm/s (17.3 cm³/min water flow rate), air velocity of 220±20 m/s (air-to-water mass ratio of 2.07), and ultrasound input power of 2.5 W: (a) nozzle position 380 μm above optimum value, and (b) 95–380 μm below optimum value.

high-velocity air, and (2) a much faster amplitude growth of the resonant capillary waves with $\lambda_C = 39$ μm, which break up to form 40-μm-diameter drops, compared to those of longer wavelengths. With resonance, the peak volume percent of the unimodal drop-size distribution occurs at a diameter determined by the third-harmonic frequency of the ultrasound ($\lambda_C = 39$ μm based on Eq. 1). To verify the resonance theory, the annulus of the air stream around the nozzle was tuned up and down from the optimum position for air impinging at the liquid jet. As shown in Figure 12, the drop-size distribution becomes broader at first, and additional peaks appear at 95 μm and 300 or 250 μm drop diameters, as the annulus is 380 μm away from the optimum position. The new peaks at 300 μm or at 250 μm can be attributed to atomization by air alone. Thus, without resonance, drop-size distributions are clearly composites of those in ultrasonic atomization and two-fluid atomization. Excellent reproducibility as shown in Figures 8–12 by the open and solid data points of the same symbols should be noted.

Comparison of experimental results to theoretical predictions of the resonant liquid capillary waves mechanism

Based on the aforementioned resonant liquid capillary waves mechanism, the calculated ζ's of the capillary waves with wavelengths of 28, 39, 85, 150 and 300 μm, and their relative values (ζ-ζ_o, choosing 85 μm capillary waves as the reference) for $\beta = 0.3$ and 0.5 are listed in Table 2. From the ζ's, temporal functions of the relative growth of amplitude scaled to its initial value, that is, $A/A_o = e^{\zeta t}$, are calculated using the 85 μm capillary waves as the reference. The results for $\beta = 0.3$ and atomization times of 50 μs and 100 μs are shown in Figure 13 as a function of air velocity for illustration. Positive ζ-ζ_o in Table 2 shows relative amplitude growth greater than one in Figure 13, indicating less stability than the reference waves; the greater the ζ-ζ_o is, the faster the relative amplitude growth increases with time. In contrast, negative ζ-ζ_o shows relative amplitude growth smaller than one, indicating better stability than the reference waves.

No significant amounts of drops larger than 300 μm diameter are produced in two-fluid atomization of water at 17.3

Table 2. ζ's of Capillary Waves Generated by Air*

V_A, m/s	λ_C, μ	ζ, s^{-1}, $\beta = 0.3$	ζ-ζ_o, s^{-1}	ζ, s^{-1}, $\beta = 0.5$	ζ-ζ_o, s^{-1}
250	28	5.33×10^5	1.75×10^5	9.55×10^5	3.52×10^5
250	39	4.87×10^5	1.29×10^5	8.47×10^5	2.44×10^5
250	85	3.58×10^5	0	6.03×10^5	0
250	150	2.75×10^5	-0.83×10^5	4.61×10^5	-1.42×10^5
250	300	1.97×10^5	-1.61×10^5	3.29×10^5	-2.74×10^5
200	28	3.01×10^5	0.77×10^5	5.69×10^5	1.89×10^5
200	39	2.91×10^5	0.67×10^5	5.19×10^5	1.39×10^5
200	85	2.24×10^5	0	3.80×10^5	0
200	150	1.74×10^5	-0.50×10^5	2.93×10^5	-0.87×10^5
200	300	1.25×10^5	-0.99×10^5	2.10×10^5	-1.70×10^5
150	28	1.22×10^5	2.0×10^3	2.71×10^5	0.64×10^5
150	39	1.39×10^5	1.9×10^4	2.66×10^5	0.59×10^5
150	85	1.20×10^5	0	2.07×10^5	0
150	150	9.59×10^4	-2.41×10^4	1.62×10^5	-0.45×10^5
150	300	6.99×10^4	-5.01×10^4	1.17×10^4	-0.90×10^5
100	28	-4.28×10^4	-8.92×10^4	6.00×10^4	-2.46×10^4
100	39	3.08×10^4	-1.56×10^4	8.60×10^4	0.14×10^4
100	85	4.64×10^4	0	8.46×10^4	0
100	150	4.02×10^4	-0.62×10^4	6.93×10^4	-1.53×10^4
100	300	3.03×10^4	-1.61×10^4	5.11×10^4	-3.35×10^4

*$\zeta = \left[\frac{\pi\beta\rho_A(V_A-u)^2}{\lambda_c\rho u} - \frac{8\pi^2\mu}{\rho\lambda_c^2}\right]$.

cm^3/min and 220 ± 30 m/s air velocity and 2.1 air-to-water-water mass ratio (see Figure 10a). This is also true for two-fluid atomization at 160 m/s air velocity and 3.24 air-to-water mass ratio (see Figure 8a). Therefore, no such large drops are expected in UMTF atomization, and capillary waves with wavelengths longer than 300 μm can be ignored at these conditions. Figure 13 shows that the ratio of the amplitude growth A/A_o in 50 μs for the 39 μm waves to that for the 85 μm waves is 90:1 at 220 m/s air velocity; the corresponding ζ-ζ_o equals 9×10^4. In addition, the ratio of the initial amplitude A_o of the 39 capillary waves to that of the 85 μm waves may be taken as 0.3 because the ratio of peak volume percent at 40 μm diameter to that at 85 μm diameter obtained in ultrasonic atomization (see Figure 6) is about 0.3:1. Therefore, only 40 μm drops are expected in UMTF atomization of water at 220 m/s air velocity. The experimental results shown in Figure 10b for UMTF atomization of 17.3 cm^3/min water at 220 ± 30 m/s air velocity and air-to-water mass ratio of 2.1 attest this expectation.

Assuming ζ-$\zeta_o = 9\times10^4$ (which yields a relative amplitude growth of 90:1 in 50 μs) in Eq. 1, the β's required at different air velocities for the 39 μm capillary waves to dominate over the 85 μm capillary waves are listed in Table 3. For comparison, β's for ζ-$\zeta_o = 7\times10^4$, which give rise to a relative amplitude growth of 33:1 in 50 μs, are also listed. This table shows that the β's required for the 39 μm capillary waves to achieve the specified ζ-ζ_o and thus the desired relative amplitude growth with respect to the 85 μm capillary waves are significantly higher (0.5–0.7 vs. 0.3–0.4) at 150–160 m/s than at 220 ± 30 m/s, indicating the requirement of a higher air-to-water mass ratio. Likewise, at 200 m/s air velocity, the ζ-ζ_o for the 39 μm capillary waves is doubled when β increases from 0.3 to 0.5. Thus, the increase of the relative amplitude growth of the 39 μm, with respect to the 85 μm, capillary waves with increasing β is consistent with the experimental results shown in Figure 9b, that is, increasing dominance of the 40 μm drops over the 85 μm drops with increasing air-to-water mass ratio.

Table 3 also shows that further reduction in air velocity to 100 m/s results in β greater than one, indicating that no drop-size distribution with predominance of the 40 μm drops can be obtained at this air velocity. Furthermore, significant amounts of drops larger than 300 μm diameter are produced in two-fluid atomization of 17.3 cm^3/min water at 100 ± 20 m/s air velocity (Figure 10a); the air-to-water mass ratio is 1.18. Therefore, capillary waves with wavelengths longer than 300 μm should also be taken into consideration in UMTF atomization at air velocities ranging from 80 to 100 m/s. Figure 13 shows that the ratio of the amplitude growth A/A_o at 100 m/s air velocity in 50 μs atomization time for the capillary waves of 39 μm, 85 μm, and 300 μm wavelengths are 0.5:1:0.5, the ratio becomes 0.2:1:0.2 as the atomization time increases to 100 μs; all are on the same order of magnitude. This is also true at β's of 0.2, 0.25, and 0.5, as shown in Table 4. This theoretical prediction is consistent with the drop-size distributions for UMTF atomization of 17.3 cm^3/min water at 100 ± 20 m/s air velocity with air-to-water mass ratio of 1.18 shown in Figure 11a and at 100 m/s air velocity with air-to-water mass ratio of 0.67 shown in Figure 11b.

Comparison of experimental results to dispersion relations

Spatial instability analysis of an incompressible semi-infinite jet of liquid with density ρ, viscosity μ, and surface tension σ, subjected to a small amplitude disturbance of $e^{-i(kz+\omega t)}$ with a fixed angular frequency ω ($\mathrm{Im}[\omega]=0$), was carried out (Leib and Goldstein, 1986) with no consideration of the effect of air based on the linearized vorticity equation (or Rayleigh equation). The undisturbed liquid jet has a radius of a and an average axial velocity of U. This analysis results in a dispersion equation for the complex wave number

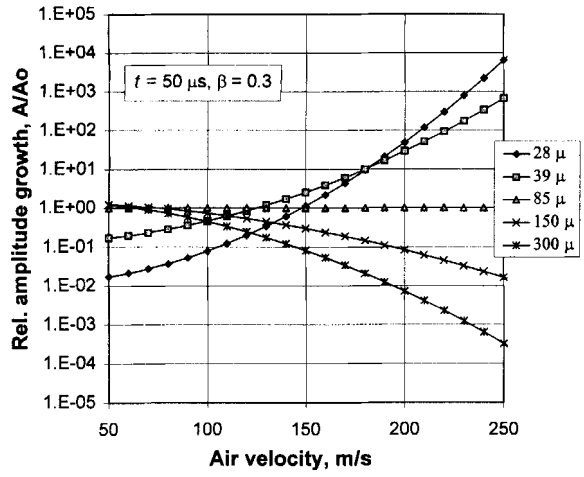

(a)

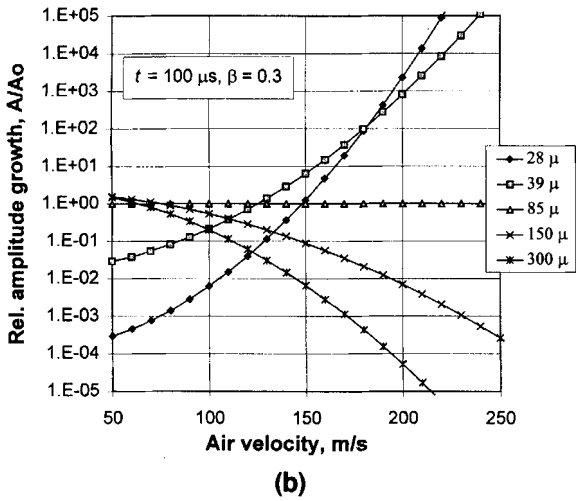

(b)

Figure 13. Temporal relative amplitude growths of capillary waves as function of air velocity at atomization times of 50 μs (a) and 100 μs (b) for surface tension of 72 dyne/cm, viscosity of 1 cp with Jeffreys sheltering parameter β of 0.3.

$k = k_r + ik_i$ as a function of a purely imaginary frequency $i\omega$; k_r equals $2\pi/\lambda$ and k_i gives growth rate, λ being the wavelength of the capillary waves. The dispersion equation shows a region of absolute instability with the Weber number ($We = \rho a U^2/\sigma$) below a critical value (0.45) and a convective instability region with the Strouhal number ($St = \omega a/U$) below the cutoff value of unity. Maximum growth rate occurs at a nondimensional wave number ($k_r a = 2\pi a/\lambda$) smaller than one and gives rise to drop diameters larger than $2a$, undisturbed diameter of the water jet. As shown in Table 5, a water jet with an undisturbed radius of 0.465 mm issuing from a vibrating nozzle at average velocities of 12 cm/s and 42 cm/s falls in the absolute instability and convective instability regimes, respectively. The unity Strouhal number requires that the externally imposed frequency is smaller than 40 Hz at 12 cm/s average water velocity and 145 Hz at 42 cm/s average water velocity. As shown in Table 5, the Strouhal numbers for the

Table 3. Jeffreys' Sheltering Parameter β's Required for Water Capillary Waves with Wavelength $\lambda = 39$ μm to Achieve the Specified $\zeta - \zeta_o$ with Respect to 85 μm Waves*

V_A, m/s	β	β
	$\zeta-\zeta_o = 7\times10^4$ s^{-1} Rel. $A(t = 50\ \mu s)/A_o = 33$**	$\zeta-\zeta_o = 9\times10^4$ s^{-1} Rel. $A(t = 50\ \mu s)/A_o = 90$**
250	0.20	0.23
220	0.25	0.3
200	0.31	0.36
160	0.49	0.58
150	0.56	0.66
100	1.31	1.55
80	2.11	2.49

*$\zeta = \left[\frac{\pi\beta\rho_A(V_A - u)^2}{\lambda\rho u} - \frac{8\pi^2\mu}{\rho\lambda^2}\right]$.

**Rel. $A(t)/A_o = \text{Exp}\,(\zeta - \zeta_o)t$.

ultrasonic frequencies used in this study are much higher. In addition, the measured drop diameters are much smaller than $2a$ (40 μm and 85 μm vs. 0.93 mm). Therefore, we believe that both the ultrasonic atomization and the UMTF atomization cannot be attributed to break up of the Rayleigh-mode capillary waves with no due consideration of the effect of air velocity in the UMTF atomization.

The effect of air on the Rayleigh-mode convective instability was carried out for both spatially growing disturbances (Lin and Lian, 1993) and temporally growing disturbances of $e^{(ikz+\omega t)}$ (Lin and Ibrahim, 1990). The resulting dispersion equations of growth rate as a function of nondimensional wave number $k_r a$ show that maximum growth rate occurs at $k_r a$ ranging from 0.6 to 0.8, which also leads to drop diameters larger than $2a$. Further, the growth rate is reduced as the Weber number increases (stabilizing effect). These theoretical predictions based on the Rayleigh-mode instability are contradictory to our experimental observations of drop diameters (much smaller than $2a$) and the destabilizing effects of the Weber number. Therefore, contribution of the Rayleigh-mode instability to the UMTF atomization is ruled out.

In contrast, temporal instability analysis of a viscous liquid jet surrounded by a viscous gas in a vertical pipe (Lin and Ibrahim, 1990) shows that Taylor-mode breakup takes place when the Weber number is much larger than the density ratio of the liquid to the gas, and the resulting drop diameters are smaller than $2a$. Furthermore, the dispersion relations show that maximum growth rate increases as the Weber number increases. Specifically, the dispersion relations for a water jet surrounded by air shows that $k_r a$, where maximum growth rate occurs, is a function of the Weber number (We), the Reynolds number (Re), and the Froude number ($Fr = U^2/ga$). $k_r a$ increases from 15 to 40 as We increases from 10^5 to 10^6 at $Re = 400$ and $Fr = 2{,}000$ (Figure 9 of Lin and

Table 4. Relative Amplitude Growth at 100 m/s Air Velocity

	$A(t = 50\ \mu s)/A_o$			$A(t = 100\ \mu s)/A_o$		
λ, μm	$\beta = 0.20$	$\beta = 0.25$	$\beta = 0.5$	$\beta = 0.20$	$\beta = 0.25$	$\beta = 0.5$
39	0.30	0.39	1.2	0.09	0.14	1.2
85	1	1	1	1	1	1
150	0.90	0.82	0.48	0.80	0.75	0.21
300	0.62	0.56	0.20	0.50	0.30	0.04

Table 5. Nondimensional Groups at Relevant Atomization Conditions of This Study

Ultrasonic Atomization of a Water Jet 0.93 mm in Diameter at Water Velocities of 12 and 42 cm/s and Ultrasonic Frequencies of 54 and 174 kHz

U, cm/s	We	Re	Fr	St @ 54 kHz	St @ 174 kHz
12	0.1	56	3.2	1.3×10^3	4.2×10^3
42	1.2	195	38.7	3.8×10^2	1.2×10^3

Two-fluid Atomization of a Water Jet 0.93 mm in Diameter at Water Velocities of 12 and 42 cm/s and Air Velocities of 100, 160, and 220 m/s

V_A, m/s	U, cm/s	$\dot{m}_A/\dot{m}_L$	V, m/s	We	Re	Fr
160	12	3.24	122	9.9×10^4	6.7×10^4	3.3×10^6
100	42	1.18	54	1.9×10^4	2.5×10^4	6.4×10^5
220	42	2.07	148	1.5×10^5	6.9×10^4	4.8×10^6

Ibrahim, 1990); it increases from 10 to 15 as Re increases from 300 to 400 at $We = 10^5$ and $Fr = 2{,}000$ (Figure 12 of Lin and Ibrahim, 1990), but decreases from 15 to 10 as Fr increases from 2,000 to 4,000 at $Re = 400$ and $We = 10^5$ (Figure 13 of Lin and Ibrahim, 1990). Similar effects of We, Re, and Fr on the maximum growth rate are predicted by this theoretical analysis. It should be noted that the Weber number defined in Lin and Ibrahim (1990) is the inverse of the Weber number used in this article.

Since one of the interfacial kinematics conditions is the continuity of the radial and tangential components of the velocity across the interface (Lin and Ibrahim, 1990), the velocity at the interface lies between the average liquid velocity U and the air velocity V_A. An average velocity V based on conservation of momentum, namely, $V = (\dot{m}_A V_A + \dot{m}_L V_L)/(\dot{m}_A + \dot{m}_L)$, is used in calculations of We, Re, and Fr for a water jet 0.093 cm in diameter. The results for two-fluid atomization at conditions shown in Figure 8a and Figure 10a are shown in Table 5. Based on the aforementioned dispersion relations by Lin and Ibrahim, $k_r a$ for the Taylor mode breakup at $We = 10^5$, $Re = 6\times10^4$, and $Fr = 5\times10^6$ is estimated to lie between 34 and 73; the pertaining capillary wavelength for a jet diameter of 0.093 cm lies between 85 μm and 40 μm. The unified theory by Lin and Lian (Figure 9 of Lin and Lian, 1990) also predicts $k_r a$ between 40 and 45; the relevant wavelength lies between 73 and 65 μm. These wavelengths are consistent with our experimental observation of peak drop diameters of 85 μm and 40 μm that are attributed to break up of capillary waves with respective wavelengths of 85 and 39 μm. The corresponding frequencies are 54 kHz and 174 kHz based on the Kelvin equation and the nozzle frequency spectrum (see Figure 4). The frequencies corresponding to the $k_r a$ from the dispersion relations are not given (Lin and Ibrahim, 1990; Lin and Lian, 1990, 1993).

Conclusions

Ultrasound has a very significant effect on the drop-size and size distribution of two-fluid or airblast atomization of a water jet. This effect can be attributed to resonance between the liquid capillary waves generated by ultrasound and those generated by high-velocity air. Specifically, capillary waves are first generated on the cone of liquid film at the nozzle tip when a water jet issues from the nozzle tip, vibrating at an ultrasonic frequency. They are magnified in amplitude downstream by air blowing around them, resulting in jet atomization with drop diameters proportional to their wavelength which is, in turn, determined by the ultrasonic frequency in accordance with the Kelvin equation. Theoretical calculations based on the two-parameter (Jeffreys sheltering parameter β and atomization time t) amplitude growth theory for such resonant liquid capillary waves give remarkable agreement with the experimental results of drop-size and size distribution. Uniform drops of diameter determined by the third-harmonic frequency of the ultrasound are obtained at high air velocity and large air-to-water mass ratio (150–160 m/s at 3.24 air-to-water mass ratio or 200 m/s at 2.1 air-to-water mass ratio). In contrast, drop-size distributions with multiple peaks are obtained at low air velocity and small air-to-water mass ratio (100 m/s and 1.2 air-to-water mass ratio). Further, the effect of air-to-water mass ratio can be accounted for by the effect of β on the relative amplitude growth of the capillary waves. These new findings provide not only a new means of controlling drop-size and size distribution in two-fluid atomization but also direct evidence of the capillary wave mechanism, possibly Taylor-mode breakup. Detailed analysis of the dispersion relations at relevant atomization conditions is needed to fill the gap between the experimental results of UMTF atomization and the theoretical instability analysis of jet breakup with externally imposed frequency in the presence of high-velocity air.

Acknowledgments

Support of this work by the National Science Foundation under grant CTS-9120807 in the Division of Chemical and Transport System is gratefully acknowledged. One of the authors (S. C. T.) also would like to acknowledge Professor Chen Tsai at the University of California, Irvine, for helpful discussions and suggestions, and Gerald Roski for assistance in obtaining the frequency spectrum.

Notation

a = radius of undisturbed liquid jet
u = wave velocity $= (2\pi\sigma/\lambda_C\rho)^{1/2}$
f = frequency of ultrasound, in Hz
g = gravitational acceleration
$\dot{m}_A$ = air-mass flow rate
$\dot{m}_L$ = liquid or water flow rate

Subscripts

A = air
L = liquid or water
C = capillary waves
r, i, o = real, imaginary, initial values

Literature Cited

Adelberg, M., "Breakup Rate and Penetration of a Liquid Jet in a Gas Stream," *AIAA J.*, **5**, 1408 (1967).

Adelberg, M., "Mean Drop Size Resulting from the Injection of a Liquid Jet into a High-Speed Gas Stream," *AIAA J.*, **6**, 1143 (1968).
Berger, H. L., "Characterization of a Class of Widely Applicable Ultrasonic Nozzles," ICLASS (1985); Sono-Tek brochure, *Ultrasonic Atomizing Nozzle Systems*, Empirial College, London, England (1991).
Dombrowski, N., and W. R. Johns, "The Aerodynamic Instability and Disintegration of Viscous Liquid Sheets," *Chem. Eng. Sci.*, **18**, 203 (1963).
Elrod, S. A., B. Hadimioglu, B. T. Khuri-Yakub, E. G. Rawson, E. Richley, and C. F. Quate, "Nozzles Droplet Formation with Focused Acoustic Beams," *J. Appl. Phys.*, **65**, 3441 (1989).
Erickson, J. J., "Ultrasonic Transducer Drive Circuit," U.S. Patent No. 4,642,581 (Feb. 10, 1987).
Eroglu, H., and N. Chigier, "Wave Characteristics of Liquid Jets from Airblast Coaxial Atomizers," *Atomization and Sprays*, **1**, 349 (1991).
Jeffreys, H., "On the Formation of Water Waves by Wind," *Roy. Soc. Proc., Series A*, **107**, 189 (1925).
Lang, R., "Ultrasonic Atomization of Liquids," *J. Acoust. Soc. Amer.*, **34**, 6 (1962).
Laskowski, J. J., and W. E. Ranz, "Spray Quenching," *AIChE J.*, **16**, 802 (1970).
Lefebvre, A. H., *Atomization and Sprays*, Hemisphere, New York (1989).
Leib, S. J., and M. E. Goldstein, "The Generation of Capillary Instabilities on a Liquid Jet," *J. Fluid Mech.*, **168**, 479 (1986); "Convective and Absolute Instability of a Viscous Liquid Jet," *Phys. Fluids*, **29**, 952 (1986).
Lin, S. P., and E. A. Ibrahim, "Instability of a Viscous Liquid Jet Surrounded by a Viscous Gas in a Vertical Pipe," *J. Fluid Mech.*, **218**, 641 (1990).
Lin, S. P., and Z. W. Lian, "Mechanisms of the Breakup of Liquid Jets," *AIAA J.*, **28**, 120 (1990).
Lin, S. P., and Z. W. Lian, "Absolute and Convective Instability of a Viscous Liquid Jet Surrounded by a Viscous Gas in a Vertical Pipe," *Phys. Fluids*, **A5**, 771 (1993).
Lin, S. P., and D. R. Woods, "A Branching Liquid Jet," *Phys. Fluids*, **A3**, 241 (1991).
Marshall, W. R., "Atomization and Spray Drying," *AIChE Chemical Engineering Progress*, Vol. 50, Monograph Series 2 (1954).
McDonell, V. G., and G. S. Samuelsen, "Structure of Vaporizing Pressure Atomized Sprays," *Atomization and Sprays*, **3**, 321 (1993).
Reitz, R. D., and F. V. Bracco, "Mechanism of Atomization of a Liquid Jet," *Phys. Fluids*, **25**, 1730 (1982).
Swithenbank, J., J. M. Beer, D. Abbott, and G. C. McCreath, "A Laser Diagnostic Technique for the Measurement of Droplet and Particle Size Distribution," Aerospace Sciences Meeting, Washington, DC (1976).
Tsai, S. C., and B. Viers, "Airblast Atomization of Viscous Newtonian Liquids Using Twin-Fluid Jet Atomizer," *ASME J. Fluid Eng.*, **114**, 113 (1992).
Tsai, S. C., "Ultrasound-Modulated Two-Fluid Atomization," U.S. Patent pending (1995).

Manuscript received Jan. 8, 1996, and revision received June 10, 1996.